Experimental results: The resonator chip was inserted into a cryostat and cooled down to 25 K. The quality factor was obtained by measuring the transmission coefficient with a

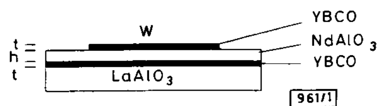

Fig. 1 *Schematic diagram of chip with five open end microstrip resonators between 8 and 100 μm width w and 6·6 and 7·4 mm length consisting of YBCO/NdAlO₃/YBCO trilayer on 10 × 10 × 0·5 mm³ LaAlO₃ substrate*

h = nominal height of the dielectric; t = film thickness; w = width of stripline

scalar network analyser. The input power was 10 dBm. The resonators were capacitively coupled by 70 μm wide coplanar microwave probes with a distance of 150 μm between the centre and two symmetric ground probes. The resonators with a width above 20 μm showed no resonances which we attributed to a shortening of the dielectric. The resonators with 14 and 8 μm width showed resonances at 4·6 GHz and at 25 K. We estimated the unloaded quality factors to be 60 and 70 with an error of 20%, respectively. The uncertainty of the quality factor measurement is due to the very weak coupling coefficient which results from the small coupling capacitors and the low quality factor of the resonators. The determination of the quality factor becomes even more difficult at higher temperatures due to the limited signal-to-noise resolution of our scalar network analyser. From these measurements the surface resistance, the attenuation constant, and the dielectric constant of the dielectric layer can be evaluated. For this configuration, radiation and dielectric losses can be neglected as compared to the conductor losses so that it can be treated as a parallel plate capacitor taking only resistive losses into account. Because the ratio w/h is large, this leads to [6]

$$Q_0 = \pi/a_c \lambda_0 = \pi\mu_0 f_0 h_{eff}/R_s$$

where a_c is the attenuation factor, λ_0 is the wavelength, f_0 the resonance frequency, h_{eff} the effective dielectric height taking into account the kinetic inductance by including the penetration depth of the magnetic field, and R_s is the surface resistance. h_{eff} was evaluated to be 730 nm in our configuration assuming a penetration depth of 150 nm. Using h_{eff}, the characteristic impedance of this parallel plate structure is 2·9 Ω for the 14 μm and 5 Ω for the 8 μm wide resonator.

The resulting surface resistance for the 8 μm resonator was 190 μΩ and the attenuation factor was 30 dB/m at 25 K. This is in good agreement with theoretical calculations which yield 25 dB/m for this configuration. The dielectric constant was determined from the resonance frequency to be 24·5. For the 14 μm wide resonator the unloaded quality factor was 60 which results in an R_s of 200 μΩ, an attenuation factor of 31 dB/m and a dielectric constant of 23·3. The errors of the surface resistance and the attenuation factor are given by the uncertainty of the quality factor measurement and thus amount to 20%. The high R_s and attenuation constant values are mainly due to the disadvantageous microstrip dimensions which result in low quality factors. As can be seen from the above equation the quality factor is linearly proportional to the effective height of the dielectric. Thus to increase the quality factor not only the film quality should be improved, but also the dielectric thickness increased. These requirements will be a challenge to materials science. Substituting $NdAlO_3$ by a dielectric with an even lower dielectric constant such as MgO or Y_2O_3 will enable higher characteristic impedance values and higher propagation velocities.

Conclusions: We have fabricated a microstrip transmission line resonator in epitaxial $YBCO/NdAlO_3/YBCO$ multilayer technology. From a transmission factor measurement we determined a quality factor of 70 at 25 K and at 4·6 GHz. The attenuation constant was evaluated to 30 dB/m and the surface resistance was 190 μΩ at 25 K. The dielectric constant of sputtered $NdAlO_3$ was 24·5. This clearly demonstrates the usefulness of this technology. Higher characteristic impedance and better film properties are now envisaged to improve the attenuation and the propagation velocities of the microstrip lines for packaging and integrated microwave circuits. Thicker dielectrics with lower dielectric constants will be necessary to achieve this goal.

Acknowledgments: The authors thank B. Sipos and F. Fox for technical assistance and E. Wolfgang for stimulating discussions. This work was partially sponsored by the German Ministry of Research and Technology under contract number 13N5812.

29th January 1992

W. Rauch*, A. A. Valenzuela and G. Sölkner (*Siemens AG, Research and Development, D-8000 München 83, Germany*)

H. Behner and G. Gieres (*Siemens AG, Research and Development, D-8520 Erlangen, Germany*)

E. Gornik (*Walter-Schottky-Institut, TU München, Am Coulombwall, D-8046 Garching, Germany*)

* Also with Siemens AG, Research and Development, D-8250 Erlangen, and Walter-Schottky-Institut, TU München, Am Coulombwall, D-8046 Garching, Germany

References

1 LEE, A. E., PLATT, C. E., BURCH, J. F., SIMON, R., GORAL, J. P., and AL-JASSIM, M. M.: 'Epitaxially grown sputtered $LaAlO_3$ films', *Appl. Phys. Lett.*, 1990, **57**, pp. 2019–2021

2 VALENZUELA, A. A., and RUSSER, P.: 'High Q coplanar transmission line resonator of $YBa_2Cu_3O_{7-x}$ on MgO', *Appl. Phys. Lett.*, 1989, **55**, pp. 1029–1031

3 POND, J. M., CAROLL, K. R., HORWITZ, J. S., CHRISEY, D. B., OSOFSKY, M. S., and CESTONE, V. C.: 'Penetration depth and microwave loss measurements with a $YBa_2Cu_3O_{7-\delta}/LaAlO_3/YBa_2Cu_3O_{7-\delta}$ trilayer transmission line', *Appl. Phys. Lett.*, 1991, **59**, pp. 3033–3035

4 BEHNER, H., GIERES, G., and SIPOS, B.: 'Characterization of sputter-deposited YBCO films by X-ray photoelectron spectroscopy', *Fresenius J. Anal. Chem.*, 1991, **341**, pp. 301–307

5 SHAREN, M. J., CARDONA, A. H., SUN, J. Z., BOURNE, L. C., and SCHRIEFFER, J. R.: 'A simple magnetization technique for determining critical currents in superconducting thin films', *Jpn. J. Appl. Phys.*, 1991, **30**, pp. L15–17

6 TABER, R. C.: 'A parallel plate resonator technique for microwave loss measurements on superconductors', *Rev. Sci. Instrum.*, 1990, **61**, pp. 2200–2206

1·57 μm InGaAsP/InP SURFACE EMITTING LASERS BY ANGLED FOCUS ION BEAM ETCHING

H. P. Lee, A. Scherer, E. D. Beebe, W. P. Hong, R. Bhat and M. A. Koza

Indexing terms: Semiconductor lasers, Lasers, Etching techniques

The characteristics of 1·57 μm InGaAsP/InP surface emitting lasers based on an in-plan ridged structure and 45° beam deflectors defined by angled focused ion beam (FIB) etching are reported. With an externally integrated beam deflector, threshold currents and emission spectra identical to conventional edge emitting lasers are achieved. These results show that FIB etching is a very promising technique for the definition of high quality mirrors and beam deflectors on semiconductor heterostructures for a variety of integrated optoelectronic devices.

The advantages of surface emitting lasers over conventional edge emitting lasers have been well documented [1]. Existing surface emitting lasers (SEL) can be classified into two categories: those with vertical cavity [1], or conventional in-plan lasers which couple light output vertically by means of 45° beam deflctors [2–4] or distributed Bragg gratings [5].

Despite rapid progress in GaAs/AlGaAs vertical cavity SELs in recent years [6], the development of InGaAsP/InP vertical cavity SELs has been hampered by the difficulty of realising high reflectivity semiconductor quarter-wavelength Bragg mirrors. For in-plan SELs, angled ion beam or reactive ion beam etching (RIE) [2, 3] and the mass transport process [4] (at 690 to 740°C) have been used to form the beam deflectors for GaAs/AlGaAs and InGaAsP/InP lasers, respectively. We report the fabrication and device characteristics of ridge InGaAsP/InP SELs with both folded-cavity [3] and external beam deflector by maskless scanning FIB etching. By avoiding high temperature mass transport treatment, this process is compatible with the fabrication of more complicated optoelectronic circuits involving transistors and detectors. It also offers greater flexibility over existing ion beam etching techniques.

The basic structure of the folded-cavity SEL is shown in Fig. 1*a*. The laser structure consists of a 0·25 μm InGaAsP

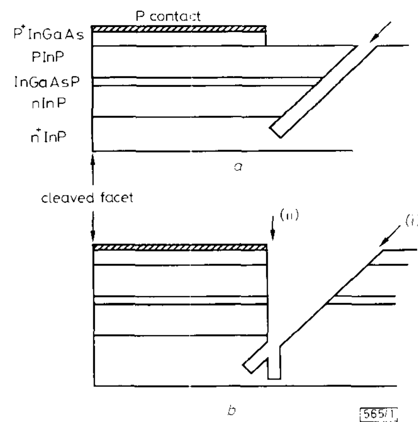

Fig. 1 *Schematic diagram of surface emitting laser structure with folded cavity and external beam deflector*

Arrows indicate locations of FIB etching
a Folded cavity
b External beam deflector

active layer ($\lambda = 1{\cdot}5\,\mu m$), a 0·1 μm InGaAsP cladding layer ($\lambda = 1{\cdot}3\,\mu m$), 2 μm *p*-doped InP cladding layer and a 0·15 μm p^+ InGaAs cap layer, all grown by low pressure MOCVD on an n^+ InP substrate. A conventional 4 μm wide ridge laser is first processed following standard procedure described in Reference 7. The stripe width is tapered to 6 μm over a distance of 5 μm near the folded cavity to reduce diffraction loss. The folded cavity is formed by FIB etching (using 25 kV Ga^+ as the ion beam source) at an angle 45° to the wafer plane and 5 μm away from the end of the *p* metal. During the FIB etching, the pattern to be removed (defined in the form of rectangular cut) is first aligned by using secondary electron image and then etched by rastering the FIB. The depth of the etched facet is controlled by the number of scans of the FIB. Fig. 2 shows the SEM picture of an etched surface. No electrical shorting of the *PN* junction is observed after etching. Finally, lasers with cavity length 300–400 μm are formed by cleaving the front facets. The continuous-wave (CW) light against current (L-I) and the emission spectrum measured at 20°C of a typical device are shown in Fig. 3*a* and Fig. 4*a*, respectively. Typically a 300 μm long edge-cleaved laser will have a threshold current I_{th} of 25–30 mA and a differential quantum efficiency of 11%. The soft turn-on on the L-I curve and multimode oscillation suggested that a large spontaneous emission component R_{sp} is present in the device [8]. This is likely caused by a higher threshold carrier density N_{th} due to diffraction loss in the folded cavity and optical loss in the unpumped region of the folded cavity between the 45° mirror and the top *p* metal. A high N_{th} also causes emission toward shorter wavelength as shown in Fig. 4*a*. To circumvent these problems, we have modified the structure by forming a verti-

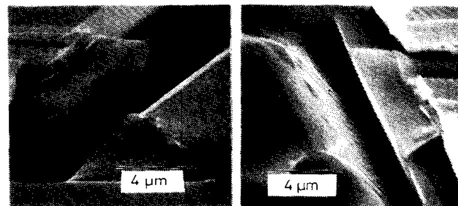

Fig. 2 *SEM micrographs on both sides of 45° mirror etch*

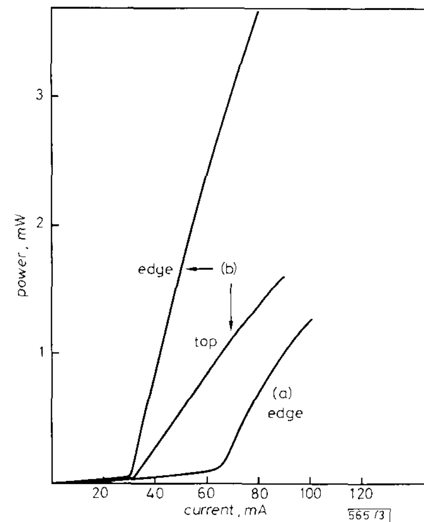

Fig. 3 *L-I curves of lasers with folded cavity and external beam deflector*

a Folded cavity
b External beam deflector

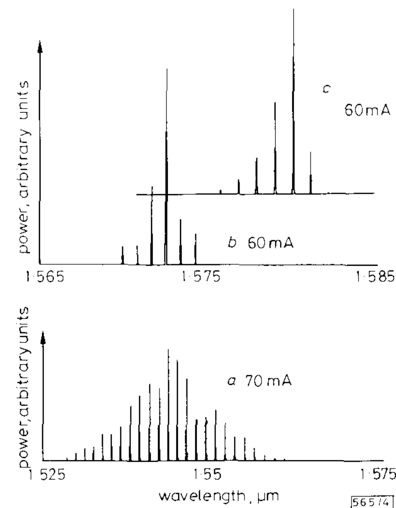

Fig. 4 *Emission spectra of laser with folded-cavity external beam deflector and edge-cleaved facets*

a Folded cavity
b External beam deflector
c Edge-cleaved facets

cal edge mirror and an external beam deflector separated by $\sim 6\,\mu m$ as shown in Fig. 1*b*. This is realised by two successive narrow, deep ($>5\,\mu m$) etches perpendicular and 45° to the wafer plan, respectively. The unwanted material in between is then 'lifted off' by etching away lateral support at both ends. The measured L-I (from front facet and top surface) and emission spectrum are shown in Fig. 3*b* and Fig. 4*b*, respectively. This device exhibits almost identical I_{th}, internal quantum efficiency and an emission spectrum to that of the edge-cleaved device, indicating that the scattering loss due to the FIB etched facet is minimum. It is also evident that the quantum efficiency from the top emission can be further improved by applying a high reflection coating on the beam deflector and by optimising the spacing between the edge mirror and the 45° deflector so that a larger fraction of light can be coupled out vertically.

Compared to mirror formation by conventional RIE, maskless FIB etching offers a number of advantages. The absence of photoresist in maskless FIB etching reduces vertical ridges along the etched surfaces caused by the roughness of the photoresist during the lithography process. Secondly, because the FIB etching process is generally nonreactive and nonselective, smooth facets can be formed on semiconductor heterostructures (waveguide, laser cavity etc) already covered with dielectric or metal films. This provides an extremely flexible way of fabricating reflectors and beam splitters with extremely narrow dimensions ($\sim 0.5\,\mu m$) only limited by resputtered material during the etching.

In summary, we have demonstrated an in-plan ridge InGaAsP/InP SELs with 45° beam deflectors by angled FIB etching with performance comparable to edge-cleaved structure. We find FIB etching to be a powerful technique for converting in-plan edge emitting lasers into surface emitting devices.

Acknowledgment: We thank E. Kapon for discussion of the work. The work is partially supported by Office of Naval Research under the contract N00014-89-C-0309.

10th December 1991

H. P. Lee, A. Scherer, E. D. Beebe, W. P. Hong, R. Bhat and M. A. Koza (*Bell Communications Research, Red Bank, New Jersey 07701, USA*)

References

1 IGA, K., KOYAMA, F., and KINOSHITA, S.: 'Surface emitting semiconductor lasers', *IEEE J. Quantum Electron.*, 1988, **24**, pp. 1845–1855

2 YANG, J. J., SERGANT, M., JANSEN, M., OU, S. S., EATON, L., and SIMMONS, W. W.: 'Surface emitting GaAlAs/GaAs linear laser array with etched mirror', *Appl. Phys. Lett.*, 1986, **49**, pp. 1138–1140

3 TAKESHI, T., COLDREN, L. A., and MERZ, J. L.: 'Lasing characteristics of a continuous-wave operated folded-cavity surface-emitting laser', *Appl. Phys. Lett.*, 1990, **56**, pp. 2267–2269

4 LIAU, Z. L., and WALPOLE, J. N.: 'Large monolithic two-dimensional arrays of GaInAsP/InP surface-emitting lasers', *Appl. Phys. Lett.*, 1987, **50**, pp. 528–530

5 KOJIMA, K., NODA, S., MITSUNAGA, K., KYUMA, K., and HAMANAKA, K.: 'Monolithic integration of an AlGaAs/GaAs multiple quantum well distributed feedback laser and a grating coupler for surface emission', *Appl. Phys. Lett.*, 1987, **50**, pp. 1705–1707

6 JEWELL, J. L., HARBISON, J. P., SCHERER, A., LEE, Y. H., and FLOREZ, L. T.: 'Vertical-cavity surface emitting lasers: design, growth, fabrication characterization', *IEEE J. Quantum Electron.*, 1991, **27**, pp. 1332–1346

7 KAMINOW, I. P., STULZ, L. W., KO, J. S., DENTAI, A. G., NEHORY, R. E., DEWINTER, J. C., and HARTMAN, R. L.: 'Low-threshold InGaAsP ridge waveguide lasers at 1·3 μm', *IEEE J. Quantum Electron.*, 1983, **19**, pp. 1312–1318

8 AGRAWAL, G. P., and DUTTA, N. K.: 'Long wavelength semiconductor lasers' (Van Nostrand Reinhold, New York, 1986), chap. 6

NEAR 100% EFFICIENT FIBRE MICROLENSES

H. M. Presby and C. A. Edwards

Indexing terms: Optical fibres, Lenses

Microlenses have been fabricated directly on the ends of optical fibres which demonstrate 90% (−0·45 dB) coupling efficiencies to semiconductor lasers. The lenses are made by laser micromachining a spinning fibre in a microlathe arrangement. Theoretically, it is possible to collect nearly 100% of the laser radiation with the aspheric lens design presented.

Introduction: Improving the coupling efficiency between a semiconductor light source and optical fibre is generally achieved by the use of a microlens formed on the end of the fibre [1]. The lens serves to match the modes of the laser and the fibre.

The most common way to fabricate microlenses is by tapering the fibre down to a point and melting the end [2]. The resulting lenses are hemispherical in shape and typically collect less than 50% (−3 dB) and at best 55% (−2·5 dB) of the available laser radiation [3].

We have designed and fabricated optimal microlenses for laser-to-fibre coupling that have achieved efficiencies of 90% (−0.45 dB). Nearly 100% coupling is theoretically achievable with this design.

Ideal lens shape: For a microlens to be ideal it must possess the following four characteristics:

(1) it should have an aperture large enough to collect all the laser radiation

(2) it should have a focal length that perfectly matches the laser and fibre modes

(3) it should be free of spherical aberration

(4) it should be appropriately coated to eliminate Fresnel reflection.

The first three conditions cannot be simultaneously satisfied by a hemispherical lens shape.

The performance of a hemispherical microlens is severely impaired by its small diameter as compared to the mode of the fibre [4]. The efficiency η of a hemispherical microlens coupled to a laser source can be considered as the product of the lens transmittivity T and coupling coefficient C.

$$\eta = T|C|^2 \tag{1}$$

T includes the power lost to Fresnel reflections and beam truncation by the finite lens aperture. The limited aperture is due to the inability of the hemispherically shaped lens to refract rays beyond a critical angle of incidence. The coupling coefficient C reveals the limited ability to couple the pure Gaussian mode of the laser with the truncated and aberrated mode of the hemispherically tipped fibre. The aberration is

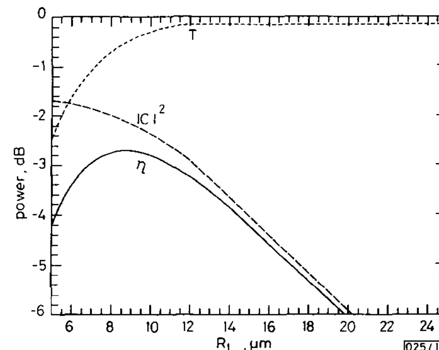

Fig. 1 *Factors limiting coupling efficiency of hemispherical microlens*